Energy conservation by group dynamics in schooling fish

Yangfan Zhang[1]*, George V. Lauder[1],

[1]Department of Organismic and Evolutionary Biology, Harvard University, 26 Oxford St, Cambridge, Massachusetts, 02138, USA

*Corresponding author. Email: yangfan_zhang@fas.harvard.edu

Short title: Energy conservation by fish schooling

Abstract

Many animals moving through fluids exhibit highly coordinated group movement that is thought to reduce the cost of locomotion. However, direct energetic measurements demonstrating the energy-saving benefits of fluid-mediated group movements remain elusive. By characterizing both aerobic and anaerobic metabolic energy contributions in schools of Giant danio (*Devario aequipinnatus*) fish, we discovered that fish schools have a *J*-shaped metabolism–speed curve, with a minimum metabolic cost at ~1 body length s^{-1}. We demonstrate that fish schools reduce total energy expenditure (TEE) per tail beat by up to 56% compared to solitary fish. When reaching their maximum sustained swimming speed, fish swimming in schools had a 44% higher maximum aerobic performance and used 65% lower non-aerobic energy for high-speed swimming compared to solitary individuals, which lowered the TEE and total cost of transport by up to 53%, near the lowest recorded for any aquatic organism. Fish in schools also recovered from exercise 43% faster than solitary fish. The non-aerobic energetic savings that occurs when fish in schools actively swim at high speed can considerably improve both peak and repeated performance which is likely to be beneficial for evading predators. These energetic savings may underlie the prevalence of coordinated group locomotion in fishes.

One-Sentence Summary: Fish schools showed a *J*-shaped metabolism-speed curve and reduced the energy use per tail beat up to 56% at high swimming speed compared to solitary fish.

Introduction

Newton's laws of motion underpin animal locomotion, from fine-scale maneuvers to long-distance migrations (*1*). As speed increases or during migration involving sustained movement over long distances, animals often move in groups: *e.g.*, migratory birds in V-formation (*2*), ducklings swimming in formation (*3*), cyclists in a peloton (*4*), elite marathon runners (*5*), and fish schools (*6*). To overcome gravitational or fluid dynamic resistance to forward motion, animals use both aerobic and glycolytic metabolism (oxidative and substrate-level phosphorylation at the cellular level) to generate energy and sustain movement in the air, on land, and in the water. In water, a fluid that is 50-times more viscous than air and contains much less O_2 per Kg than air, the need for aquatic animals to reduce fluid dynamic drag for energy conservation is even greater than for aerial or terrestrial locomotion. Here we use fish schooling behaviour as a model system to explore how the fluid dynamics of group movement can enable energetic savings compared to locomotion by a solitary individual. Fish schooling behaviours are some of the most prominent social and group activities exhibited by aquatic vertebrates.

Fish may school for many reasons, including foraging, reproduction, and migration, and fish schools often exhibit high-speed movement during evasion from predators. Hence, natural selection can put pressure on the formation of schools and individual interactions within a school. Besides 'safety in numbers' where individuals in a large school have a lower probability of becoming prey, can there be more concrete energetic benefits of high-speed swimming as a school? Since fluid drag scales as velocity squared (*7*), movement at higher speeds places a premium on mechanisms to conserve energy. Fast and unsustainable swimming is fueled by aerobic metabolism with a major contribution from anaerobic glycolysis (*8*) (*9*). During high-speed swimming aerobic capacity is maximized (*9*), and energy use is more likely to compete

with other activities than in low-speed swimming which only occupies a small portion of aerobic capacity. The direct consequences of unsustainably engaging anaerobic glycolysis include both fatigue and metabolic perturbation (such as changing blood acidity) that need time to recover after bouts of intense locomotion. Animals become vulnerable during recovery because of their hindered ability to repeat peak locomotor performance in the presence of predators.

Another reason to experimentally evaluate the energetic cost of group locomotion in fishes is that endurance and efficiency are often key to achieving lifetime fitness, especially in fish species that undergo significant migrations. Fish groups usually undergo long-distance migrations at a slow speed of 0.5-1.0 BL s^{-1} as recorded by tags on migrating fish (Fig. S1). The common migratory speed of ~1 BL s^{-1} for marine and anadromous fish could be related to the minimum cost of transport (*10*). However, there is currently no direct measurement of the absolute costs of teleost fish swimming demonstrating a minimum group metabolic rate ($\dot{M}O_2$) at an optimal speed (U_{opt}). Fish schools in nature swim over a wide range of speeds (Fig. S1) but no study has directly characterized the total energy expenditure (TEE), and accounted for the potentially substantial anaerobic metabolic costs involved in higher speed locomotion. As a result, the swimming TEE performance curve of fish schools from the minimum swimming speed to the critical swimming speed (U_{crit}) has not yet been measured.

More broadly, despite the widespread notion that group motion saves energy (*6*), very few studies have directly measured the energetic cost of group movement and compared the cost of movement by solitary individuals. In the canonical case of V-formation flight in birds, energetic saving is exclusively inferred from indirect measurements, *e.g.,* heart rate (*2*), and flapping frequency and phase (*11*) (Table 1). There are no direct measurements of group metabolic energy consumption, and indeed this would be extremely challenging to accomplish. Although some energetic aspects of schooling fishes have been studied (*12*) (*13*) (*14*) (*15*) (*16*),

these studies have analyzed a limited range of speeds and focused on aerobic metabolism (*see* Table 1). In fact, several field and laboratory kinematic studies suggest that both bird flocks and fish schools do not always conserve aerobic energy (*16*) (*17*) (*18*) and indicate that moving in a group can actually involve *increased* costs. Without directly measuring the energetic cost of movement, inferences solely based on kinematics do not include complex group interactions, and the interaction between collective behaviour and fluid dynamics. Consequently, we do not yet have a holistic and mechanistic view of where and how the collective movement might conserve energy.

For swimming fishes, fluid dynamic experiments have shown how collective movement can improve swimming efficiency due to interactions among deforming bodies and through interactions between moving animals and the local fluid environment, and we summarize these proposed energy-saving mechanisms in Figure 1. Our current understanding of energy saving mechanisms during collective locomotion in fishes is largely based on computational fluid dynamic models with a few analyses using robotic systems (*6*) (*18*) (*19*) (*20*) (*21*), but the link between such models and fish metabolic energy saving is not established. We expect that the need to conserve energy in animals moving against air or water resistance should be greater at higher speeds, and we hypothesize that fish in schools may be able to reduce the total cost of high-speed locomotion relative to solitary movement, leading to reduced non-aerobic energetic costs and time of recovery for schooling fish swimming at speeds occupying the majority (> 50%) of their aerobic capacity. Our secondary objective is to determine the differences (if any) between the swimming performance curves (metabolism versus speed) of solitary fish and fish schools.

To evaluate these hypotheses, we directly measured both the aerobic and non-aerobic energy used by schooling fishes over a wide range of water velocities (0.3–8.0 body lengths s^{-1};

BL s^{-1}), and then compared the swimming performance curve to that of solitary fish. We equipped a high-resolution (*see* Methods for our approach to enhancing the signal-to-noise ratio in our respirometer) swim-tunnel respirometer with two orthogonal high-speed cameras to quantify three-dimensional (3-D) fish kinematics. This enabled us to simultaneously measure energetics, 3-D dynamics of fish schools (n=5 replicate schools), and the kinematics of solitary fish (n=5) of a model species, giant danio (*Devario aequipinnatus*), that exhibits an active directional group swimming from near still water to maximum sustained speeds (equivalent to a Reynolds number range of $6.4 \bullet 10^3$ to $1.8 \bullet 10^5$; Fig. S2), using a U_{crit} test.

Results

We discovered that both solitary fish and fish schools have a *U*-shaped aerobic metabolic rate ($\dot{M}O_2$)-speed curve over the lower portion of their speed range (0.3–3 BL s^{-1}, Fig. 2A, D). Fish schools swimming at ~1.0 BL s^{-1} consume less energy than at slower speeds ($F_{9,40} = 24.7$, $p \leq 0.0007$), while swimming at 3 BL s^{-1} consumes a similar amount of energy to maintain position at a water velocity of 0.3 BL s^{-1} ($p = 0.85$; Fig. 2D). Danio schools have a minimum aerobic cost ($\dot{M}O_{2min}$ = 212.9 mg O_2 kg^{-1} h^{-1}) at 1.25 BL s^{-1}. $\dot{M}O_{2min}$ at this optimal speed (U_{opt}) was *lower* than both the $\dot{M}O_2$ of aggregating behaviours (328.5 mg O_2 kg^{-1} h^{-1}) exhibited before U_{crit} test (Table S1, Fig. S3) and for the group at rest in still water $\dot{M}O_2$ (267.9 mg O_2 kg^{-1} h^{-1}) (by 35% and 21% respectively; $F_{2,12} = 16.7$, $p \leq 0.02$, Fig. 2A,B). Swimming at U_{opt} reduces the energetic cost below that of swimming at either slower or higher speeds. Indeed, the Strouhal number of fish schools decreased from 2.1 at the lowest speed to 0.3 at the energetic minimum U_{opt}, and then increased to 0.4 at the higher U_{crit}.

We also characterized the kinematic features that result in elevated $\dot{M}O_2$ at low water velocities. Danio maintaining balance in low-velocity aggregations had a higher tail beat

143 frequency (f_{TB}) than solitary fish ($F_{1,80} \geq 9.8$, $p \leq 0.002$). However, at U_{opt} and the highest speed
144 of active directional schooling, fish in schools had a lower f_{TB} ($F_{1,80} \geq 4.6$, $p \leq 0.035$) than
145 solitary fish (Fig. 4B). The 3-D angular heading of schooling fish transitioned from
146 omnidirectional to pointing against water flow when water velocity is above 0.75 BL s^{-1}, and
147 individual fish orient into the flow starting at 0.3 BL s^{-1} (Fig. 4C). Although the body angle and
148 turning frequency of solitary fish and schools decreased with water velocity, schooling fish had a
149 higher turning frequency ($F_{1,80} \geq 15.6$, $p < 0.002$) below 0.75 BL s^{-1} than solitary fish (Fig.
150 4D,E).

151 We discovered that, across the entire 0.3–8 BL s^{-1} range, $\dot{M}O_2$-speed curves of fish
152 schools are *J*-shaped (reached 1053.5 mg O_2 kg^{-1} h^{-1} at 8 BL s^{-1}) whereas solitary fish showed an
153 *S*-shaped curve (reaching a plateau of 760.2 mg O_2 kg^{-1} h^{-1} & ~10% CV in 6–8 BL s^{-1}; Fig. 2C),
154 demonstrating that schooling dynamics results in a 44% higher maximum aerobic performance
155 ($F_{1,80} = 30.0$, $p < 0.001$). This increased maximum aerobic performance translated to a lower use
156 of aerobic capacity compared to solitary fish over 0.3–8 BL s^{-1} (*see* the discussion for how fish
157 swimming in school can improve aerobic performance). Collectively, fish schools used a 36%
158 lower proportion of their aerobic scope than solitary fish (Wilcoxon test: $p = 0.0002$, Fig. 2F).
159 Fish schools used a 38% lower proportion of aerobic scope (34 vs. 55%) at 4 BL s^{-1} (50% U_{crit}
160 & > 50% aerobic scope onward), and consistently used ~25% lower proportion of their aerobic
161 scope at 6 and 7 BL s^{-1} than solitary fish ($F_{1,103} \geq 4.8$, $p \leq 0.03$, Fig. 2E).

162 Given that fish schools had a higher maximum aerobic performance, generally used a
163 lower proportion of their aerobic scope, and individuals within the schools have a 14% lower f_{TB}
164 than the solitary fish at 8 BL s^{-1} (11.5 vs. 13.3 Hz, $F_{1,80} = 15.1$, $p < 0.001$), we predicted that fish
165 schools, compared with solitary fish, use less anaerobic energy to supplement aerobic energy for
166 the high-speed movement approaching their aerobic limit. Hence, we measured post-exercise O_2

167 utilization, a majority of which is used to restore high-energy phosphate storage and
168 glycolytically induced metabolic perturbations (EPOC: Excess Post-exercise O_2 Consumption).
169 We discovered that fish schools have a 65% lower EPOC (0.69 vs. 1.95 mg O_2; $t_8 = 4.5$, $p =$
170 0.0021), and recover 43% faster than solitary fish (8 vs. 14 h; $t_8 = 2.8$, $p = 0.025$; Fig. 2G, H).
171 To estimate the relative proportions of aerobic and anaerobic energy contributions for
172 locomotion at each swimming speed, we modeled EPOC in addition to $\dot{M}O_2$, the aerobic cost (>
173 50% U_{crit} & aerobic scope, Fig. 3A) (Table S2). We also estimated the total O_2 cost during the
174 entire swimming process for each school and individual and calculated total energy expenditure
175 (TEE) (*9*). The TEE of fish schools was 38–53% lower than that of the solitary fish between 5–8
176 BL s^{-1} ($F_{1,103} \geq 7.4$, $p \leq 0.008$; Fig. 3D). TEE of fish schools was only 42–143 % higher than the
177 aerobic metabolic rate at 5–8 BL s^{-1} ($F_{1,96} \geq 3.5$, $p \leq 0.001$) and anaerobic metabolic energy only
178 accounted for 29–58 % of the TEE depending on speed (Fig. 3B). In contrast, TEE of solitary
179 fish was 131–465 % higher than the aerobic metabolic rate between 5–8 BL s^{-1} ($F_{1,112} \geq 10.7$, $p \leq$
180 0.001), where anaerobic energy accounted for 62–81% of the TEE depending on speed (Fig. 3C).
181 Schooling dynamics reduced the total cost (aerobic plus anaerobic) of transport (TCOT)
182 by an average of 43% compared to swimming alone ($F_{1,103} = 6.9$, $p = 0.01$), and most of this
183 energy conservation happens at higher speeds when fish approach their aerobic limit. Schooling
184 dynamics in danio enables an extremely shallow rate of increase in TCOT with speed compared
185 to that of an individual (Fig. 3E). The TCOT of solitary fish increased by 490% (6.5 kJ km^{-1} kg^{-}
186 ^{1}) at 8 BL s^{-1}, whereas the schooling TCOT increased by only 200% (3.6 kJ km^{-1} kg^{-1}) at 8 BL s^{-}
187 ^{1}. Therefore, individual fish form a more energy-efficient biological entity when they collectively
188 move as a school.
189 To answer the question of how schooling dynamics reduces TEE, we combine video
190 analysis of fish tail beat kinematics with simultaneous aerobic and anaerobic measurements to

compute energy expended *per tail beat* (TEE•*beat*$^{-1}$), and compared values for fish in schools to those for solitary fish. Schooling fish reduced TEE•beat^{-1} by 30–56% at higher speeds compared to solitary fish ($F_{1,81} \geq 7.3$, $p \leq 0.008$), a substantial reduction in TEE•beat^{-1} consumed both by the school, and by individual fish within a school (Fig. 4A). Notably, the energetic benefits during active directional schooling occur when fish schools become more streamlined, as school length increased with speed and plateaued beyond 2 BL s^{-1} (Fig. 4F), while the 3-D distance among individuals stayed relatively constant at ~1.2 BL (Fig 4G). These results directly demonstrate schooling dynamics benefits the swimming kinematics of individual fish within the school and results in a net outcome of up to 53% TEE reduction in fish schools compared to solitary fish.

Discussion

Simultaneous characterization of energetics and kinematics enable an integrated understanding of both the physiology and physics of fish schooling behaviour. Hydrodynamic models, kinematic measurements, and robotic analyses of fish groups indicate that the cost of swimming can be reduced when fish swim beside neighbouring fish (*18*), behind or in front of another fish (*22*), or behind leading individuals (*6*) (Fig. 1). We have demonstrated here that fish schools downshifted an overall *J*-shaped swimming energetics curve at higher speeds by ~43%, regardless of the position of individual fish when swimming in a group. This considerable energy savings occurs even though danio regularly move within the school and do not maintain stable inter-individual positions. We expect that this is due to the fact that there are a number of different hydrodynamic mechanisms that fish can use to save energy within a school (Fig. 1) and thus energetic savings by collective motion does not require either fixed positional arrangements among individuals or specific kinematic features (such as tail beat synchronization) compared to

solitary locomotion. Based on these data, we regard fish schooling as a highly robust behaviour that provides considerable energetic benefits that are not sensitive to specific fish locations or movements. Energy saving occurs through a drastic reduction in non-aerobic energy contribution when fish approach aerobic limits. One of the key ecological benefits of reduced use of glycolysis is a faster recovery time from fatigue (Fig. 2H), which would enable fish schools in nature to repeat high-performance movements. Considering that high-speed maneuvers are extremely common in predatory evasion (*23*) and food-searching group motion (*24*), the energy saving of fish schooling at high speed and the faster recovery that followed can have a considerable impact on the fitness outcome (*25*) (*26*).

Schooling dynamics enhances aerobic performance and reduces anaerobic energy use

We discovered a significant amount of energy conservation for active directional swimming occurring at speeds above 3 BL s^{-1}. In nature, fish schools routinely exhibit active directional group locomotion above ~6 BL s^{-1} (Fig. S1, Table S3) (*27*), a speed that engages anaerobic glycolysis. And yet there are no previous measurements of the anaerobic cost of schooling in fish. Hence, key previously unrecognized benefits of active directional group swimming are (1) increased aerobic performance, (2) a reduced use of aerobic capacity and anaerobic energy, and (3) a resultant faster recovery from the associated metabolic perturbations and costs of swimming at higher speeds.

We present direct evidence of substantial non-aerobic energy saving by demonstrating the 65% lower EPOC (Fig. 2G) used by fish that swam in schools. Anaerobic glycolysis is crucial in permitting continued movement when aerobic limits are reached at high swimming speeds (*28*). Often vertebrates at higher speeds use more fast twitch fibers that generate high-frequency contractile force in part through anaerobic glycolysis (*29*) (*30*). The higher EPOC for

239 single fish is unlikely to have been confounded by any possible stress effect of swimming as a
240 solitary fish. Stressed solitary fish would have elevated aerobic metabolic rates in low water
241 velocity, which we show is not the case for our experiments (*see* Fig 2D). Indeed, to mitigate the
242 stress response, we acclimated fish to the solitary conditions and habituated fish to the
243 respirometer for a quiescent day before the experiment (*see* more details in experimental animal
244 and protocols). Moreover, after the highest swimming speeds followed by an active recovery
245 process immediately following, fish likely prioritize exercise performance and recover the
246 essential functions (speedy recovery allows fish to restore their swimming performance) (*31*)
247 (*32*) (*33*). As a result, we observed a TEE being ~2.5 fold higher than the aerobic metabolic
248 energy expenditure which agrees with the theoretical estimates based on individual yearling
249 sockeye salmon (*34*).

250 To present a complete energetic profile showing the total energy expenditure (TEE) of
251 locomotion for fish schooling, we model the non-aerobic cost (EPOC) on top of the aerobic
252 swimming performance curve. The model is rooted in the use of aerobic and glycolytic energy
253 when fish swim above 50% U_{crit} (*35*) and a commonly observed inflection point of faster
254 anaerobic end-product accumulation is at ~50% aerobic scope (*8*) (*see* Methods for detailed
255 physiological bases and criteria for EPOC modeling). This model elucidates how aerobic and
256 anaerobic metabolic energy constitute TEE, fuel muscles, generate locomotor thrust and
257 overcome hydrodynamic drag during swimming.

258 Fish swimming at higher speeds (> 50% U_{crit}) routinely exhibit a burst-&-glide gait (*33*,
259 *35*). The repeated bursting is fueled by anaerobic glycolysis and the gliding phase enables peak
260 $\dot{M}O_2$ (*36*) to replenish the venous O_2 content (*37*). Fish within a school are known to increase
261 gliding time and decrease burst time by 19% when they are trailing the leading fish (*38*), *e.g,* a
262 lower f_{TB} of fish schools at 8 BL s^{-1} is related to the extended gliding time (Fig. 4B). We reason

263 that the higher proportion of time spent gliding likely enables more bouts of peak $\dot{M}O_2$ and
264 enhances the maximum aerobic performance (*36*) (*37*). This enhanced maximum aerobic
265 performance enables fish to use a lower proportion of their aerobic scope for locomotion.
266 Physiological studies of exercise metabolism and locomotion suggest that a lower proportional
267 use of aerobic scope during movement relates to a reduced accumulation of anaerobic end-
268 products (*8*). Collectively, our results showed that the increased aerobic performance (Fig. 2C)
269 and the reduced use of the aerobic capacity (Fig. 2E) for swimming above 50% U_{crit} in fish
270 schools likely played a key role in reducing the use of glycolysis and the accumulation of lactate
271 (*e.g.* EPOC, Fig. 2G) for high-speed swimming (*9*, *33*).
272 We also demonstrated that the need for energy saving in fish schools at lower speeds (< 3
273 BL s^{-1} or 38% U_{crit} Fig. 2E, 3D,E) is not as crucial as at higher speeds where we demonstrated
274 substantial energy savings in the schools compared to solitary individuals. Fluid drag is
275 exponentially less at lower speeds compared to higher speeds. Fish predominately use aerobic
276 metabolism to support low-speed steady speed swimming for prolonged periods (*9*) which does
277 not require lengthy recovery as swimming at higher speeds where glycolysis contributes to
278 energy needs. The costs of low-speed swimming are often less than < 20% of aerobic capacity
279 (Fig. 2E), which leaves the majority of aerobic capacity (>50%) for other activities. Therefore,
280 the benefits of reducing the energetic cost of locomotion are likely not major factors underlying
281 behaviours such as low-speed milling (*39*) and aggregation (*40*) in fishes, where other ecological
282 drivers such as collective feeding and reproduction likely dominate the fitness landscape.
283
284 **Schooling dynamics and energy conservation**
285 Our 3D kinematic analyses shed some light on the complex interactions between
286 schooling and hydrodynamics that enables energy saving by fishes moving in groups. One of the

key possible mechanisms is local interactions among individuals, where the kinematics of individual fish respond to the wakes shed by neighbours (*41*). Kinematic and simulation studies indicate that 2–3 coordinated fish can save energy (*42*) (*18*) through local interactions. We directly demonstrated that eight coordinated fish can save energy and recent simulations show that schooling benefits can extend to at least 23 fish (*19*). Although these studies appear to suggest that the energetic benefits of schooling are scalable, we are still some ways from proving the exact mechanisms of how the large school size in nature is coordinated and whether or not local interactions are still one of the mechanisms for energy saving when scaling up school size.

We show that danio in a school keep a relatively consistent 3-D distance from neighbours and have small variation in mean position even as individuals routinely change position within the school (Fig. 4G). Computational fluid dynamic analyses of fish schools show that a small 3D neighbouring distance (*e.g.* < 0.4 BL s^{-1}) increases drag and can increase swimming costs, whereas a large 3-D neighbouring distance (*e.g.* > 2 BL s^{-1}) reduces the hydrodynamic benefits (*42*). There may thus be an optimal mean distance among individuals within a school to maximize energetic savings. Whether inter-individual distance should change as swimming speed increases remains an open question.

To encapsulate the complex interaction among animal physiology, kinematics and fluid dynamics, more comprehensive quantification beyond simple kinematic metrics are necessary. For example, the wing flapping frequency of birds in a V-formation can be higher than for solitary flight despite strong indirect evidence of overall energy saving by V-formation flying (*2*) (*11*) (*17*), and flapping phase of adjacent birds may be informative for understanding the fluid dynamic advantages of V-formation flying (*11*). Likewise, phase matching of body motion between neighbouring fish can help individual fish within the school to boost thrust or reduce drag (*18*). Fish can also adjust their body stiffness and maintain f_{TB} while reducing the amount of

311 muscle activity needed to generate movement (*43*) (*44*) (*45*). Thus, we did not observe consistent
312 and substantial changes in the f_{TB} of fish within the schools compared to solitary swimmers
313 despite demonstrating substantial energetic savings by the group at high speed. Although
314 reduced f_{TB} has been used in past studies as an indirect indicator of energy saving in fishes (*46*),
315 we caution that f_{TB} is not necessarily an indicator of energy use in group dynamics where fish
316 constantly and dynamically interact with complex vortices and flow generated by other
317 individuals. By simultaneously measuring kinematics and energetics, we discovered a
318 downshifted *J*-shaped performance curve of TEE per tail beat in fish schools at higher speeds
319 (Fig. 4A), even with limited alteration in f_{TB} at lower swimming speeds within the school. This
320 suggests that the locomotor muscle fibres in the body musculature of fish within the school need
321 to generate less force as indicated by the lower measured TEE. Fish can possibly fine-tune
322 undulatory motion to harness kinetic energy from nearby vortices (*18*) (*42*), reducing biological
323 energy contribution for thrust.
324

325 **Aerobic metabolic rate–speed curve of fish schools**

326 We discovered that the aerobic metabolic rate ($\dot{M}O_2$)–speed curve is *U*-shaped (Fig. 2D)
327 at speeds less than 3 BL s^{-1}, but *J*-shaped across the entire locomotion speed range of the species.
328 Swimming at 0.3 BL s^{-1} costs the same energy as moving at 3 BL s^{-1}. Regardless of the exact
329 shape of the curve, the essence of our finding is that fish schools can manifest a minimal absolute
330 energetic cost ($\dot{M}O_2$) at a mean group swimming speed of ~1.0 BL s^{-1} which is higher than the
331 minimum swimming speeds tested. Thus, fish schools can swim at a speed with the least amount
332 of energy use and potentially extend the distance travelled with the same amount of metabolic
333 substrate onboard. This swimming speed of minimum cost closely matches the migratory speeds
334 of carangiform and subcarangiform migratory fishes (often as schools) which are in the range of

335 0.5 to 1.5 BL s^{-1} as recorded by tags on migrating fish (*47*, *48*) (Fig. S1; Tables S1, S3).
336 Although *D. aequipinnatus* is not a migratory species, our results suggest that the migratory
337 speed of fish schools likely occurs at the speed showing the minimum aerobic metabolic rate for
338 long-distance locomotion. Indeed, the Strouhal number when fish schools swim at U_{opt}, showing
339 a minimum aerobic energy cost of locomotion, is 0.3, a hallmark of efficient swimming for many
340 fish species (*49*). Fish of different size swimming at 1 BL s^{-1} will necessarily move at different
341 Reynolds numbers, and hence the scaling of body size to swimming speed needs to be
342 considered in the future but is beyond the scope of this current study.

343 The exact energetic mechanisms underpinning the chosen migratory speeds of fish
344 schools would benefit from more in-depth studies. Since both fish schools and solitary
345 individuals have U_{opt} of ~1 BL s^{-1}, the $\dot{M}O_2$–speed curve of a fish school might be the average of
346 individual curves from fish within the school. However, pushing and pulling forces from
347 hydrodynamic interactions of neighbouring fish can help swimmers settle into stable
348 arrangements, a phenomenon known as the Lighthill conjecture (*50*). Further studies will need to
349 explore whether individuals within the school are more frequently located at points
350 recommended by the Lighthill conjecture which could potentially result in minimum metabolic
351 costs of locomotion at U_{opt} in fish schools. Research on fish swimming in large aquaculture
352 circular tanks has discovered that holding a large school of salmonids at a water velocity of ~1
353 BL s^{-1} resulted in healthy growth and good conditions (*51*). This phenomenon seems to suggest
354 that the minimum metabolic costs of locomotion yield the largest available aerobic capacity for
355 growth and other functions.

356 Higher locomotion costs at the lowest speeds are likely caused by the higher postural
357 costs for active stability adjustments in the near-still fluid. The direct link between higher
358 energetic costs caused by a higher 3-D body angle and higher turning frequency at the lowest

speeds in solitary danio (Fig. 4D, E) supports previous results in skates (*52*) where energetic costs are high at the very lowest swimming speeds due to the increased energetic cost involved in maintaining body stability and generating lift in negatively buoyant fishes. We expect more species that move in the fluid to show a higher postural cost in near-still fluid but careful measurements of both body kinematics and position along with high-resolution respirometry will be required to demonstrate this phenomenon in a diversity of fish species. Elevated costs should be indicated at the lowest speeds as a direct increase in $\dot{M}O_2$ and not just as COT. When the denominator for deriving COT is less than 1, COT tends to skew towards the higher value at the lowest speeds. Mechanistically, fish at low fluid speeds have lower muscle and propeller efficiencies (*34*) with reduced fluid-assisted stability. Increased active stability adjustments such as fin movements (*52*) and tilting behaviours that enable the fish's body to act as a hydrofoil (*53*) are used for stability control (see supplementary video). Danio do not show intermittent swimming gaits at low speeds as observed in some labriform swimmers (*54*) (*55*), and hence gait-specific kinematics most likely do not play a role in the elevated locomotion cost that we observe at the lowest speeds. As fish move more rapidly over a speed range, we note that the total cost of transport of ~1.2 kJ km^{-1} kg^{-1} at 3 BL s^{-1} is among the lowest recorded for aquatic organisms, and is less than the TCOT (1.5 kJ km^{-1} kg^{-1}) for jellyfish (the most energetically efficient low-speed swimmers) (*4*) swimming at < 2 BL s^{-1} (*56*).

In summary, our experiments on Giant danio have demonstrated substantial energy conservation resulting from schooling dynamics across a wide range of speeds. Direct measurement of both aerobic and non-aerobic energy use is critical for understanding the rapid collective movement of animals in groups. Fish schooling in the high-drag viscous aquatic medium serves as a model for understanding how group movement by animals can be a more

energy-efficient biological collective than movement by isolated individuals. By increasing maximum aerobic performance, fish schools save anaerobic energy and reduce the recovery time after peak swimming performance. Furthermore, by decreasing the proportion of metabolic capacity and recovery time devoted to locomotion, animals can apportion more energy to other fitness-related activities, such as digestion, growth and reproduction. More broadly, comprehending how the collective dynamics of animal movements in the water, land, and air can modify the energy use profiles of individuals can provide a better understanding of the ecological and evolutionary implications of group locomotion.

Materials and Methods

Experimental animals

The experiments were performed on giant danio (*Devario aequipinnatus*) that were acquired from a local commercial supplier near Boston, Massachusetts USA (Table S4). Five schooling groups are randomly distributed and housed separately in five 37.9 l aquaria (n=8 per tank). The five solitary individuals are housed separately in five 9.5 l aquaria (n=1 per tank). The individual housing condition acclimated the single *D. aequipinnatus* to the solitary environment and helped to reduce any isolation stress that might elevate the whole-organism metabolic rate. In fact, the aerobic locomotion cost of solitary individuals showed no statistical difference from (in fact, being numerically lower) that of fish schools at a very low testing speed. The flow speed is similar to some areas of the aerated home aquarium for each individual fish. This suggests that the stress of solitary fish likely does not meaningfully contribute to the higher locomotor costs (*see* experimental protocol for more details on mitigating the stress). The condition factor showed no difference between solitary fish and fish schools (0.81 vs. 0.99; $t_8 = 2.14$, $p = 0.065$). All aquaria have self-contained thermal control (28 °C), an aeration system (>95 % air

407 saturation, % sat.) and a filtration system. Water changes (up to 50% exchange ratio) were
408 carried out weekly. Fish were fed *ad libitum* daily (TetraMin, Germany). Animal holding and
409 experimental procedures were approved by the Harvard Animal Care IACUC Committee
410 (protocol number 20-03-3).
411

412 **Integrated Biomechanics & Bioenergetic Assessment System (IBBAS)**

413 The core of our Integrated Biomechanics & Bioenergetic Assessment System (IBBAS) is a
414 9.35-l (respirometry volume plus tubing) customized Loligo® swim-tunnel respirometer (Tjele,
415 Denmark). The respirometer has an electric motor, and a sealed shaft attached to a propeller
416 located inside the respirometer. Regulating the revolutions per minute (RPM) of the motor
417 controls water velocity of the tunnel. The linear regression equation between RPM and water
418 velocity (V) is established ($V = 0.06169 \bullet RPM – 5.128$, $R^2 = 0.9988$, $p < 0.0001$) by velocity
419 field measured by particle image velocimetry (PIV). Hence, the aerobic costs during locomotion
420 are measured through the regulation of the water velocity.

421 The swim-tunnel respirometer is oval-shaped. The central hollow space of the respirometer
422 increases the turning radius of the water current. As a result, the water velocity passing the cross-
423 section of the swimming section (80 × 80 × 225 mm) is more homogenous (validated by direct
424 particle image velocimetry (PIV) of flow in the working section of the respirometer following
425 the procedures in (*57*)). Moreover, a honeycomb flow straightener (80 × 80 × 145 mm) is
426 installed in the upstream section of the swimming section that was specifically designed to create
427 relatively uniform flow across the working section (also confirmed by direct flow imaging).
428 Based on our flow visualization analyses, the effective distance of slow-moving fluid due to
429 boundary layer was <2.5mm at speeds above 2 BL s^{-1}. The boundary layer played ever
430 diminishing role at higher speeds (> 4 BL s^{-1}) when energy saving of fish schools becomes more

predominant. Danio (~10 mm wide) cannot effectively hide in the narrow boundary layer. In addition, the convex hull volume of the fish school did not change as speed increased, suggesting that the fish school was not flattening against the wall of the swim tunnel, a typical feature when fish schools are benefiting from wall effects. In nature, fish in the centre of the school effectively swim against a 'wall' of surrounding fish where they can benefit from hydrodynamic interactions with neighbours.

To standardize the experimental apparatus and avoid instrument variation, solitary fish and fish schools are measured in the same swim-tunnel respirometer, and the same overall experimental design is used as in previous studies (*13*) (*12*) (*14*). The ratios of respirometer:individual volume (r_{RI}) were between 1116–8894, whereas r_{RI} in our system was 2200 (we also used a larger solitary *D. aequipinnatus* to increase the signal-to-noise ratio). An optimal r_{RI} is essentially a balance of giving enough space for fish to exhibit a natural burst-&-glide gait and generating a reliable signal-to-noise ratio to measure the decline of dissolved O_2 (DO) in water (*58*). The increase in the signal-to-noise ratio can come from the better technology of the O_2 probe (we used an optical O_2 probe which has a higher measurement sensitivity than the Winkler method or Electrode & Galvanic probes used in the previous studies, *see* (*59*) for review) and modifications to the swim-tunnel respirometer. Herein, a water loop is installed 95 cm downstream of the propeller and water is returned to the respirometer 240 cm upstream of the swimming section. Flow in the water loop moves (produced by an in-line circulation pump, Universal 600, EHEIM GmbH & Co KG, Deizisau, Germany) in the same direction as the water flow in the swimming tunnel. A high-resolution fibre optic O_2 probe (Robust oxygen probe OXROB2, PyroScience GmbH, Aachen, Germany) is sealed in the loop in the downstream of the circulation pump where there is better mixing to continuously measure the DO level in the water (recording frequency ~1 Hz, response time < 15s). The designated water sampling loop together

with the water mixing by the propeller and water pumps effectively reduces the noise-to-signal ratio. As a result, the respirometry system reaches a stable signal-to-noise ratio once the sampling window is longer than 1.67 mins (*see* Fig. S6), well within the duration of the velocity step to obtain a stable signal-to-noise ratio for calculating $\dot{M}O_2$ (*36*).

The oxygen probe was calibrated to anoxic (0 % sat., a solution created by super-saturated sodium sulphite and bubbling nitrogen gas) and fully aerated water (100 % sat.). After fish removal, the background $\dot{M}O_2$ in the swim-tunnel respirometer was measured for a 20-min sealed period before and after each trial to calculate the average background $\dot{M}O_2$ (< 6% of fish $\dot{M}O_2$), which was used to correct for the $\dot{M}O_2$ of fish (*58*). The pre-filtered water (laboratory grade filtration system) is constantly disinfected by UV light (JUP-01, SunSun, China) located in an external water reservoir to suppress the growth of microbial elements. Water changes of 60% total volume occurred every other day and a complete disinfection by sodium hypochlorite is conducted weekly (Performance bleach, Clorox & 1000 ppm).

To simultaneously measure schooling dynamics and swimming kinematics, the customized oval-shaped swim-tunnel respirometer is located on a platform with an open window beneath the swimming section. The platform is elevated 243 mm above the base to allow a front surface mirror to be installed at a 45° angle. This mirror allows a high-speed camera (FASTCAM Mini AX50 type 170K-M-16GB, Phontron Inc., United States, lens: Nikon 50mm F1.2, Japan) to record the ventral view. The second camera (FASTCAM Mini AX50 type 170K-M-16GB, Phontron Inc., United States, lens: Nikon 50mm F1.2, Japan) is positioned 515 mm to the side of the swimming section to record a lateral view. Synchronized lateral and ventral video recordings were made at 125 fps, and each frame was 1024 by 1024 pixels. To avoid light refraction passing through the water and distorting the video recordings, the swim-tunnel respirometry is not submerged in the water bath. Temperature regulation of the respirometer is achieved by

479 regulating room temperature, installing thermal insulation layers on the respirometer and
480 replenishing the water inside the respirometer from a thermally regulated (28 °C, heater: ETH
481 300, Hydor, United States & chiller: AL-160, Baoshishan, China) water reservoir (insulated
482 37.9-l aquarium) located externally.

483 The aerated (100% sat., air pump: whisper AP 300, Tetra, China) reservoir water is flushed
484 (pump: Universal 2400, EHEIM GmbH & Co KG, Deizisau, Germany) to the respirometer
485 through an in-line computer-controlled motorized ball valve (U.S. Solid) installed at the in-flow
486 tube. The other in-line one-way valve is installed at the out-flow tube. The out-flow tube is also
487 equipped with a one-way valve. The valve is shut during the measurement period, a
488 precautionary practice to eliminate the exchange of water between the respirometer and the
489 external reservoir when the water moves at a high velocity inside the respirometer. This flushing
490 was manually controlled to maintain DO above 80 % sat. Every time the respirometer was closed
491 to measure $\dot{M}O_2$, the water temperature fluctuates no more than 0.2 °C. The water temperature
492 inside the respirometer is measured by a needle temperature probe (Shielded dipping probe,
493 PyroScience GmbH, Aachen, Germany) sealed through a tight rubber port of the respirometer.

494 To allow fish to reach the undisturbed quiescent state during the trial (another stress
495 mitigation practice), the entire IBBAS is covered by laser blackout sheet (Nylon Fabric with
496 Polyurethane Coating; Thorlabs Inc, New Jersey, United States). The room lights are shut off
497 and foot traffic around IBBAS is restrained to the absolute minimum. Fish are orientated by dual
498 small anterior spots of white light (lowest light intensity, Model 1177, Cambridge Instruments
499 Inc, New York, United States) for orientation (one to the top and the other to the side) of the
500 swimming section. The test section is illuminated by infrared light arrays.

501

502 **Experimental Protocol**

503 The energy use of vertebrates at lower speeds is primarily aerobic, while for high-speed
504 movement anaerobic metabolic pathways are activated to supply the additional (largely shorter-
505 term) energy needs (*8*). While whole-animal aerobic metabolism is measured by oxygen (O_2)
506 uptake rate ($\dot{M}O_2$), the non-aerobic O_2 cost (mostly through high-energy phosphate and
507 anaerobic glycolysis) is measured as excess post-exercise O_2 consumption (EPOC)(*9*). Both
508 metabolic energy sources contribute to the total energy expenditure (TEE) required for
509 movement. For a given workload, the higher the maximum aerobic performance of the animal,
510 the less the need for the anaerobic energy contribution (*8*, *28*). The experimental protocol
511 captures both metabolic energy contributions by measuring $\dot{M}O_2$ during locomotion and EPOC
512 afterwards.

513 We studied five replicate schools and five replicate individuals. Swimming performance test
514 trials were conducted with *Devario aequipinnatus* fasted for 24 hours, a sufficient period for a
515 small size species at 28 °C (*i.e.* high resting $\dot{M}O_2$) to reach an absorptive state. In fact, we
516 observed no specific dynamic action, the amount of O_2 consumed for digestion during the first
517 diurnal cycle (Fig. S3). Prior to the swimming performance test, testing fish were gently
518 weighted and placed in the swim-tunnel respirometer. The fish swam at 35% U_{crit} for 30 mins to
519 help oxidize the inevitable but minor lactate accumulation during the prior handling and help fish
520 become accustomed to the flow conditions in the swim-tunnel respirometer (*32*). After this time,
521 the fish to be tested were habituated (>20 hours) to the respirometer environment under quiescent
522 and undisturbed conditions. The long habituation period also helps to reduce the stress and
523 further reduce the likelihood that the solitary fish might be more stressed than the fish schools
524 and showed an elevated $\dot{M}O_2$ (*12*). During this time, we used an automatic system to measure the
525 resting $\dot{M}O_2$ for at least 19 hours. Relays (Cleware GmbH, Schleswig, Germany) and software
526 (AquaResp v.3, Denmark) were used to control the intermittent flushing of the respirometer with

527 fresh water throughout the trial to ensure O_2 saturation of the respirometer water. $\dot{M}O_2$ was
528 calculated from the continuously recorded DO level (at 1 Hz) inside the respirometer chamber.
529 The intermittent flow of water into the respirometer occurred over 930 s cycles with 30 s where
530 water was flushed into the respirometer and 900 s where the pumps were off and the
531 respirometer was a closed system. The first 240 s after each time the flushing pump was turned
532 off were not used to measure $\dot{M}O_2$ to allow O_2 levels inside the respirometer to stabilize. The
533 remaining 660 s when the pumps were off during the cycle were used to measure $\dot{M}O_2$. The in-
534 line circulation pump for water in the O_2 measurement loop stayed on throughout the trial.

535 We characterize the aerobic costs for the swimming performance of fish using an
536 established incremental step-wise critical swimming speed (U_{crit}) test (*9*). The first preliminary
537 trial determined the U_{crit} of this population of *Devario aequipinnatus* as 8 BL s^{-1}. Characterizing
538 the swimming performance curve required a second preliminary trial to strategically select 10
539 water velocities (0.3, 0.5, 0.8, 1.0, 1.3, 1.5, 1.8, 2.3, 2.8 BL s^{-1}) to bracket the hypothesized *U*-
540 shaped metabolism-speed curve at the lower speed (< 40% U_{crit}). Additional five water velocities
541 (3.8, 4.9, 5.9, 6.9, 8.0 BL s^{-1}) are used to characterize the exponentially increasing curve to the
542 maximum and sustained swimming speed, U_{crit} (*see* Fig. S4). Altogether, 14 points provide a
543 reliable resolution to characterize the swimming performance curve. The cross-section of the
544 danio school is ~10% of the cross-sectional area of the swim tunnel, hence the blocking effect is
545 negligible (*60*). At each water velocity, fish swam for 10 mins (*52*) to reach a steady state in
546 $\dot{M}O_2$ at low speeds (*see* Fig. S5). Above 40% U_{crit}, $\dot{M}O_2$ can become more variable (*36*). Hence,
547 in this protocol, we focus on measuring the sustained aerobic energy expenditure by calculating
548 the average $\dot{M}O_2$ for each 10-min velocity step using Eqn 1. At the 5th min of each velocity step,
549 both ventral and lateral-view cameras are triggered simultaneously to record 10-sec footage at
550 125 frames per second, at 1/1000 shutter speed and 1024 ×1024 pixel resolution. Thus, both data

551 streams of $\dot{M}O_2$ and high-speed videos are recorded simultaneously. The U_{crit} test is terminated
552 when 12.5% of fish in the school or a solitary individual touches the back grid of the swimming
553 section for more than 20 secs (*32*). The U_{crit} test lasted ~140 mins and estimates the aerobic
554 portion of TEE over the entire range of swimming performance.

555 To measure the contribution of non-aerobic O_2 cost, where the majority of the cost is related
556 to substrate-level phosphorylation, and to calculate the TEE for swimming over the entire speed
557 range, we measured EPOC after the U_{crit} test for the ensuing 19 hours, recorded by an automatic
558 system. Most previous measurements of EPOC have used a duration of ~5 hours (*see* review
559 (*31*)), but our extended measurement period ensured that longer duration recovery O_2
560 consumption during EPOC was measured completely as fish were exercised to U_{crit} (*see*
561 summary table in *16*). The intermittent flow of water into the respirometer occurred over 30 s to
562 replenish the DO level to ~95% sat. For the following 900 s the flushing pump remained closed,
563 and the respirometer becomes a closed system, with the first 240 s to allow O_2 saturation inside
564 the respirometer to stabilize. The remaining 660 s when the flushing pump was off during the
565 cycle were used to measure $\dot{M}O_2$ (*see* Eqn 1). The cycle is automated by computer software
566 (AquaResp v.3) and provided 74 measurements of $\dot{M}O_2$ to compute EPOC. Upon the completion
567 of the three-day protocol, the school or individual fish are returned to the home aquarium for
568 recovery. The fish condition was closely monitored during the first 48 hours after the
569 experiment, during which no mortality was observed.

570

571 **Bioenergetic measurement and modeling**

572 To estimate the steady-rate whole-animal aerobic metabolic rate, $\dot{M}O_2$ values were
573 calculated from the sequential interval regression algorithm (Eqn. 1) using the DO points
574 continuously sampled (~1 Hz) from the respirometer.

575 $$\dot{M}O_2 = \left[\frac{d_{DO_{[i,(i+a)]}}}{d_{t_{[i,(i+a)]}}} \bullet \left(V_r - V_f\right) \bullet S_O\right] / (t \bullet M_f) \quad \text{(Eqn. 1)}$$

576

577 Where d_{DO}/d_t is the change in O_2 saturation with time, V_r is the respirometer volume, V_f is

578 the fish volume (1 g body mass = 1 ml water), S_o is the water solubility of O_2 (calculated by

579 AquaResp v.3 software) at the experimental temperature, salinity and atmospheric pressure, t is a

580 time constant of 3600 s h^{-1}, M_f is fish mass, and a is the sampling window duration, i is the next

581 PO_2 sample after the preceding sampling window.

582 To account for allometric scaling, the $\dot{M}O_2$ values of solitary fish were transformed to match

583 the size of the individual fish in the school (*see* Table S4) using an allometric scaling exponent

584 (b = 0.7546). The calculation of the scaling relationship [$Log_{10}(\dot{M}O_2) = b \bullet Log10(M) + Log10(a)$,

585 where M is the body mass & a is a constant] was performed by least squares linear regression

586 analysis ($y = 0.7546 \bullet x + 0.2046$; $R^2 = 0.6727$, $p < 0.0001$) on the 180 data points of metabolic

587 rate and body mass from a closely related species (the best available dataset to our knowledge) .

588 (The mass scaling for tail beat frequency was not conducted because of the lack of data for *D.*

589 *aequipinnatus* and its related species. Using the scaling exponent of distant species for mass

590 scaling of tail beat frequency will introduce errors of unknown magnitude.) The allometrically

591 scaled $\dot{M}O_2$ values were used to derive other energetic metrics (listed below & such as aerobic

592 scope) for the solitary fish. The energetic metrics of fish schools are calculated from the mass-

593 specific $\dot{M}O_2$.

594 The resting oxygen uptake ($\dot{M}O_{2rest}$), the minimum resting metabolic demands of a group of

595 fish or a solitary individual, is calculated from a quantile 20% algorithm (*63*) using the $\dot{M}O_2$

596 estimated between the 10th–18th hour and beyond the 32nd –51st hour of the trial. These are the

597 periods of quiescent state when fish completed the EPOC from handling and swimming test.

598 The $\dot{M}O_2$ for the aggregation (Fig. 1B, $\dot{M}O_{2aggregate}$) is calculated as the average value using
599 the $\dot{M}O_2$ estimated between the 10th–18th hour without the effects of any tests.
600 Minimum oxygen uptake ($\dot{M}O_{2min}$) is the lowest $\dot{M}O_2$ value recorded in the entire trial,
601 which always occurred at the optimal speed when a school of fish collectively reached the lowest
602 $\dot{M}O_2$ value.
603 Active oxygen uptake ($\dot{M}O_{2active}$) is the highest average $\dot{M}O_2$ when fish are actively
604 swimming (*9*).
605 The aerobic scope (the metric for aerobic capacity) is the numerical difference between
606 $\dot{M}O_{2active}$ and $\dot{M}O_{2min}$ (*i.e.* $\dot{M}O_{2active} - \dot{M}O_{2min}$) (*9*).
607 The percentage of aerobic scope (% aerobic scope) is calculated by normalizing the $\dot{M}O_2$
608 value at a water velocity as a % aerobic scope [($\dot{M}O_2 - \dot{M}O_{2min}$) / ($\dot{M}O_{2active} - \dot{M}O_{2min}$)]. The
609 apportioning of aerobic scope to swimming performance is computed across the entire range of
610 swim speeds.
611 The excess post-exercise oxygen consumption (EPOC) is an integral area of $\dot{M}O_2$ measured
612 during post-exercise recovery, from the end of U_{crit} until reached $\dot{M}O_{2rest}$ plus 10% or within 24
613 hours post-exercise, whichever endpoint occurred first (*61*). This approach reduces the likelihood
614 of overestimating EPOC due to any potential spontaneous activities (*61*). To account for the
615 allometric scaling effect, we used the total amount of O_2 consumed (mg O_2) by the standardized
616 body mass of fish (1.66 g) for fish schools and solitary fish.
617 We model EPOC (*i.e.* non-aerobic O_2 cost) and $\dot{M}O_2$ during U_{crit} to estimate a *total* O_2 cost
618 over the duration of the swimming performance test. Our conceptual approach was pioneered by
619 Brett (*9*) in fish (*64*) and is also used in sports science (*8*). Mathematical modeling of EPOC and
620 $\dot{M}O_2$ during swimming was applied to study the effects of temperature on the total cost of
621 swimming for migratory salmon (*32*). We improved the mathematical modeling by applying the

following physiological and physics criteria. The first criterion is that significant accumulation of glycolytic end-product occurred when fish swimming above 50% U_{crit} (*33*) which corresponds to > 40% $\dot{M}O_{2max}$ (or ~ 50% aerobic scope) (*8*). This is also when fish start unsteady-state burst-&-glide swimming gait (*33*). The second criterion is that the integral area for the non-aerobic O_2 cost during swimming can only differ by ≤ 0.09% when compared to EPOC. The non-aerobic O_2 cost during swimming is the area bounded by modeled $\dot{M}O_2$ and measured $\dot{M}O_2$ as a function of time when fish swim > 50% U_{crit} (*see* Fig. 2A & Table S2). The third criterion is that total energy expenditure is expected to increase exponentially with swimming speed (Fig. S7). Specifically, these curves were fitted by power series or polynomial models, the same models that describe the relationship between water velocity and total power and energy cost of transport (Fig. S7). Following these criteria, the non-aerobic O_2 cost at each swimming speed is computed by a percentage (%) modifier based on the aerobic O_2 cost (Table S2). The exponential curve of total O_2 cost as swimming speed of each fish school or solitary individual was derived by an iterative process until the difference between non-aerobic O_2 cost and EPOC met the 2nd criterion. The sum of non-aerobic O_2 cost and aerobic cost gives the total O_2 cost.

Total energy expenditure (TEE) is calculated by converting total O_2 cost to kJ × kg^{-1} using an oxy-calorific equivalent of 3.25 cal per 1 mg O_2 (*65*).

Cost of transport (COT), in kJ × km^{-1} × kg^{-1} is calculated by dividing TEE by speed (in km × h^{-1}) (*52*).

Three-dimensional kinematic data extraction from high-speed videography

We used two synchronized 10-sec high-speed videos (lateral and ventral views, at each speed) for kinematic analyses. We calibrated the field of view of the high-speed cameras using a direct linear transformation for three-dimensional (3-D) kinematic reconstruction (DLTdv8)(*66*)

by applying a stereo calibration to the swimming section of the respirometer (*see* Fig. S8). We digitized the anatomical landmarks of fish (*see* Fig. S9) to obtain the X, Y, and Z coordinates for each marker at the 1st sec, 5th sec and 10th sec for videos recorded at each speed. These coordinates are used to calculate the following kinematic parameters. All the calculations are validated on the known length and angle of test objects inserted into the tank working section.

The 3-D distance between the tip of the nose of each fish in the school per frame is calculated in vector Eqn. 2

$$d = \sqrt{(Xa - Xb)^2 + (Ya - Yb)^2 + (Za - Zb)^2} \quad \text{(Eqn. 2)}$$

Where spatial coordinates of two neighbouring fish are (X_a, Y_a, Z_a) and (X_b, Y_b, Z_b) respectively.

The 3-D angle of each fish in the school to the frontal plane per frame is calculated by Eqn. 3

$$\theta = \arccos \frac{(X2-X1)\cdot(X3-X1)+(Y2-Y1)\cdot(Y3-Y1)+(Z2-Z1)\cdot(Z3-Z1)}{\sqrt{(X2-X1)^2\cdot(Y2-Y1)^2\cdot(Z2-Z1)^2}\cdot\sqrt{(X3-X1)^2\cdot(Y3-Y1)^2\cdot(Z3-Z1)^2}} \quad \text{(Eqn. 3)}$$

where the spatial coordinates of the caudal peduncle, nose of fish and right angle crosshair between the peduncle and the nose are (X_1, Y_1, Z_1), (X_3, Y_3, Z_3) and (X_2, Y_2, Z_2) respectively (*see* Fig. S9).

The fish's angle to water flow per frame is calculated using the arctangent function in Excel (Microsoft, United States) using the spatial coordinates of the caudal peduncle and nose of the fish.

The school length (in *X*-axis) is calculated as a 3-D distance (Eqn. 2) between the nose of the first fish of the school to the caudal peduncle of the last fish in the school.

The values (3-D distance of the individuals, 3-D body angle, 3-D school length) calculated above were averaged among the three frames at each speed as a representative kinematic feature

669 of the schools (or solitary fish) for each speed. The standard deviation of the angle to water flow
670 in fish schools is calculated from the angular values of the individuals.

671 Tail beat frequency (f_{TB}), in Hz, is calculated as the number of tail beats observed within
672 one second. We sampled 10 tail beats from fish exhibiting steady-state swimming to obtain an
673 average and representative f_{TB} for each solitary fish at each speed. We sampled 10 tail beats of
674 steady-state swimming for three individuals in the center of the fish school for an average and
675 representative f_{TB} for each fish school.

676 Turning frequency is the total number of events when fish made a 90˚ turn in the 10-sec
677 video. To make the total number of turns per individual and fish schools comparable (multiple
678 individuals inevitably have a larger absolute number of turns), we derived the average turning
679 frequency per schooling fish by dividing the total number of turns of fish school by the number
680 of fish in the school.

681 Total energy expenditure per tail beat (kJ kg^{-1} $beat^{-1}$) is calculated by TEE • $(f_{TB} \cdot 60)^{-1}$ to
682 estimate the total metabolic energy spent to achieve one stride length.

683 Additional calculations of fluid dynamic metrics were:

684 Strouhal number = (f_{TB} • tail beat amplitude) • U^{-1} (*7*). Tail beat amplitude is measured as
685 the average distance of five peak-to-peak oscillation amplitudes of the tip of the fish's tail. The
686 measurement is conducted on the calibrated high-speed video in video analysis software
687 (Phontron FASTCAM Viewer 4, Photron USA, Inc.).

688 Reynolds number = (water density • U • fish fork length) • water dynamic viscosity $^{-1}$ (*7*).
689 Water density and dynamic viscosity are given at 28 °C.

690

691 **Statistical analyses**

Measurement points are presented as mean ± s.e.m. For the metrics that failed normality tests, logarithm transformations were applied to meet the assumptions of normality of residuals, homoscedasticity of the residuals, and no trend in the explanatory variables. Since fish schools exhibit the features of a coherent functional unit, the statistical model treated one school as one sample size, and the experiment measured five replicates of fish schools. The majority of statistical comparisons used the General Linear Model (Fixed factors: solitary fish vs. fish schools & swimming speed, the label of solitary fish & fish schools as a random effect) with Holm–Šídák *post-hoc* tests. The few comparisons that used other statistical models are listed below. The comparison of $\dot{M}O_{2min}$ at U_{opt}, $\dot{M}O_2$ of aggregating behaviours exhibited at the lowest speed ($\dot{M}O_{2aggregate}$) and resting $\dot{M}O_2$ ($\dot{M}O_{2rest}$) in fish schools used one-way ANOVA with Holm–Šídák *post-hoc* tests. The comparison of EPOC between solitary fish and fish schools used a two-tailed Student's t-test. The comparison of the duration of EPOC between solitary fish and fish schools used a two-tailed Student's t-test. The overall difference in percentage aerobic scope (% aerobic scope) between fish schools and solitary individuals is compared by the Wilcoxon singed-rank test over the entire range of 14 swimming speeds. The statistical analyses were conducted in SPSS v.28 (SPSS Inc. Chicago, IL, USA). The best-fitting regression analyses were conducted using Prism v.9.4.1 (GraphPad Software, San Diego, CA, USA). 95% C.I. values were presented for all regression models as shaded areas around the regression or data points. Statistical significance is denoted by *, **, ***, **** for p-values of ≤ 0.05, ≤ 0.01, ≤ 0.001, ≤ 0.0001 respectively.

References and Notes

1. A. Biewener, S. Patek, *Animal Locomotion* (Oxford University Press, 2018).

2. H. Weimerskirch, J. Martin, Y. Clerquin, P. Alexandre, S. Jiraskova, Energy saving in flight formation. *Nature*. **413**, 697–698 (2001).

3. F. E. Fish, Kinematics of ducklings swimming in formation: Consequences of position. *Journal of Experimental Zoology*. **273**, 1–11 (1995).

4. B. Blocken, T. van Druenen, Y. Toparlar, F. Malizia, P. Mannion, T. Andrianne, T. Marchal, G.-J. Maas, J. Diepens, Aerodynamic drag in cycling pelotons: New insights by CFD simulation and wind tunnel testing. *Journal of Wind Engineering and Industrial Aerodynamics*. **179**, 319–337 (2018).

5. I. Shinichiro, Aerodynamic effects by marathon pacemakers on a main runner. *Transactions of the Japan Society of Mechanical Engineers Part B*. **73**, 1975–1980 (2007).

6. D. Weihs, Hydromechanics of fish schooling. *Nature*. **241**, 290–291 (1973).

7. S. Vogel, *Life in Moving Fluids: The Physical Biology of Flow - Revised and Expanded Second Edition* (Princeton University Press, 2020).

8. J. Laforgia, R. T. Withers, C. J. Gore, Effects of exercise intensity and duration on the excess post-exercise oxygen consumption. *Journal of Sports Sciences*. **24**, 1247–1264 (2006).

9. J. R. Brett, The respiratory metabolism and swimming performance of young sockeye salmon. *J. Fish. Res. Bd. Can.* **21**, 1183–1226 (1964).

10. F. W. H. Beamish, "Swimming capacity" in *Fish Physiology* (London: Academic Press, W.S. Hoar and D. J. Randall., 1978; https://cir.nii.ac.jp/crid/1571135650623593984), vol. VII, pp. 101–187.

11. S. J. Portugal, T. Y. Hubel, J. Fritz, S. Heese, D. Trobe, B. Voelkl, S. Hailes, A. M. Wilson, J. R. Usherwood, Upwash exploitation and downwash avoidance by flap phasing in ibis formation flight. *Nature*. **505**, 399–402 (2014).

12. F. R. Parker Jr., Reduced metabolic rates in fishes as a result of induced schooling. *Transactions of the American Fisheries Society*. **102**, 125–131 (1973).

13. M. V. Abrahams, P. W. Colgan, Risk of predation, hydrodynamic efficiency and their influence on school structure. *Environ Biol Fish*. **13**, 195–202 (1985).

14. E. Burgerhout, C. Tudorache, S. A. Brittijn, A. P. Palstra, R. P. Dirks, G. E. E. J. M. van den Thillart, Schooling reduces energy consumption in swimming male European eels, Anguilla anguilla L. *Journal of Experimental Marine Biology and Ecology*. **448**, 66–71 (2013).

15. M. Currier, J. Rouse, D. J. Coughlin, Group swimming behaviour and energetics in bluegill Lepomis macrochirus and rainbow trout Oncorhynchus mykiss. *Journal of Fish Biology*. **98**, 1105–1111 (2021).

16. M. Hvas, F. Oppedal, Influence of experimental set-up and methodology for measurements of metabolic rates and critical swimming speed in Atlantic salmon Salmo salar. *Journal of Fish Biology*. **95**, 893–902 (2019).

17. B. L. Partridge, T. J. Pitcher, Evidence against a hydrodynamic function for fish schools. *Nature*. **279**, 418–419 (1979).

18. J. R. Usherwood, M. Stavrou, J. C. Lowe, K. Roskilly, A. M. Wilson, Flying in a flock comes at a cost in pigeons. *Nature*. **474**, 494–497 (2011).

19. L. Li, M. Nagy, J. M. Graving, J. Bak-Coleman, G. Xie, I. D. Couzin, Vortex phase matching as a strategy for schooling in robots and in fish. *Nat Commun*. **11**, 5408 (2020).

20. J. Kelly, Y. (潘宇) Pan, A. Menzer, H. (董海波) Dong, Hydrodynamics of body–body interactions in dense synchronous elongated fish schools. *Physics of Fluids*. **35**, 041906 (2023).

21. F. E. Fish, C. M. Schreiber, K. W. Moored, G. Liu, H. Dong, H. Bart-Smith, Hydrodynamic performance of aquatic flapping: Efficiency of underwater flight in the Manta. *Aerospace*. **3**, 20 (2016).

22. M. Kurt, K. W. Moored, Flow interactions of two- and three-dimensional networked bio-inspired control elements in an in-line arrangement. *Bioinspir. Biomim.* **13**, 045002 (2018).

23. K. D. Jones, C. M. Dohring, M. F. Platzer, Experimental and computational investigation of the Knoller-Betz effect. *AIAA Journal*. **36**, 1240–1246 (1998).

24. J. D. Stewart, A. Barroso, R. H. Butler, R. J. Munns, Caught at the surface: myctophids make easy prey for dolphins and devil rays. *Ecology*. **99**, 1894–1896 (2018).

25. T. J. Pitcher, A. E. Magurran, I. J. Winfield, Fish in larger shoals find food faster. *Behav Ecol Sociobiol*. **10**, 149–151 (1982).

26. K. E. Jain, A. P. Farrell, Influence of seasonal temperature on the repeat swimming performance of rainbow trout Oncorhynchus mykiss. *Journal of Experimental Biology*. **206**, 3569–3579 (2003).

27. P. E. Holder, C. M. Wood, M. J. Lawrence, T. D. Clark, C. D. Suski, J.-M. Weber, A. J. Danylchuk, S. J. Cooke, Are we any closer to understanding why fish can die after severe exercise? *Fish and Fisheries*. **23**, 1400–1417 (2022).

28. O. A. Misund, A. Aglen, Swimming behaviour of fish schools in the North Sea during acoustic surveying and pelagic trawl sampling. *ICES Journal of Marine Science*. **49**, 325–334 (1992).

29. G. A. Gaesser, G. A. Brooks, Metabolic bases of excess post-exercise oxygen consumption: a review. *Med Sci Sports Exerc*. **16**, 29–43 (1984).

30. B. C. Jayne, G. V. Lauder, New data on axial locomotion in fishes: How speed affects diversity of kinematics and motor patterns. *American Zoologist*. **36**, 642–655 (1996).

31. L. C. Rome, P. T. Loughna, G. Goldspink, Temperature Acclimation: Improved Sustained Swimming Performance in Carp at Low Temperatures. *Science*. **228**, 194–196 (1985).

32. Y. Zhang, G. Claireaux, H. Takle, S. M. Jørgensen, A. P. Farrell, A three-phase excess post-exercise oxygen consumption in Atlantic salmon Salmo salar and its response to exercise training. *Journal of Fish Biology*. **92**, 1385–1403 (2018).

33. C. G. Lee, A. P. Farrell, A. Lotto, S. G. Hinch, M. C. Healey, Excess post-exercise oxygen consumption in adult sockeye (Oncorhynchus nerka) and coho (O. kisutch) salmon following critical speed swimming. *Journal of Experimental Biology*. **206**, 3253–3260 (2003).

34. S. J. Peake, A. P. Farrell, Postexercise Physiology and Repeat Performance Behaviour of Free-Swimming Smallmouth Bass in an Experimental Raceway. *Physiological and Biochemical Zoology*. **78**, 801–807 (2005).

35. P. Webb PW;, Hydrodynamics and Energetics of Fish Propulsion. *Bulletin of the Fisheries Research Board of Canada*. **Bulletin 190** (1975) (available at https://scholarworks.umass.edu/fishpassage_journal_articles/569).

36. S. J. Peake, A. P. Farrell, Fatigue is a behavioural response in respirometer-confined smallmouth bass. *Journal of Fish Biology*. **68**, 1742–1755 (2006).

37. Y. Zhang, M. J. H. Gilbert, A. P. Farrell, Finding the peak of dynamic oxygen uptake during fatiguing exercise in fish. *Journal of Experimental Biology*. **222** (2019), doi:10.1242/jeb.196568.

38. A. P. Farrell, S. M. Clutterham, On-line venous oxygen tensions in rainbow trout during graded exercise at two acclimation temperatures. *Journal of Experimental Biology*. **206**, 487–496 (2003).

39. F. E. Fish, J. F. Fegely, C. J. Xanthopoulos, Burst-and-coast swimming in schooling fish (Notemigonus crysoleucas) with implications for energy economy. *Comparative Biochemistry and Physiology Part A: Physiology*. **100**, 633–637 (1991).

40. A. Costanzo, C. K. Hemelrijk, Spontaneous emergence of milling (vortex state) in a Vicsek-like model. *J. Phys. D: Appl. Phys.* **51**, 134004 (2018).

41. R. A. Rountree, Association of Fishes with Fish Aggregation Devices: Effects of Structure Size on Fish Abundance. *Bulletin of Marine Science*. **44**, 960–972 (1989).

42. S. Camazine, J.-L. Deneubourg, N. R. Franks, J. Sneyd, G. Theraula, E. Bonabeau, *Self-Organization in Biological Systems* (Princeton University Press, 2020; https://www.degruyter.com/document/doi/10.1515/9780691212920/html).

43. S. Verma, G. Novati, P. Koumoutsakos, Efficient collective swimming by harnessing vortices through deep reinforcement learning. *Proceedings of the National Academy of Sciences*. **115**, 5849–5854 (2018).

44. D. N. Beal, F. S. Hover, M. S. Triantafyllou, J. C. Liao, G. V. Lauder, Passive propulsion in vortex wakes. *Journal of Fluid Mechanics*. **549**, 385–402 (2006).

45. J. C. Liao, D. N. Beal, G. V. Lauder, M. S. Triantafyllou, The Kármán gait: novel body kinematics of rainbow trout swimming in a vortex street. *J Exp Biol*. **206**, 1059–1073 (2003).

46. D. Quinn, G. Lauder, Tunable stiffness in fish robotics: mechanisms and advantages. *Bioinspir. Biomim.* **17**, 011002 (2021).

47. S. Marras, S. S. Killen, J. Lindström, D. J. McKenzie, J. F. Steffensen, P. Domenici, Fish swimming in schools save energy regardless of their spatial position. *Behav Ecol Sociobiol*. **69**, 219–226 (2015).

48. B. A. Block, D. Booth, F. G. Carey, Direct Measurement of Swimming Speeds and Depth of Blue Marlin. *Journal of Experimental Biology*. **166**, 267–284 (1992).

49. B. A. Block, S. L. H. Teo, A. Walli, A. Boustany, M. J. W. Stokesbury, C. J. Farwell, K. C. Weng, H. Dewar, T. D. Williams, Electronic tagging and population structure of Atlantic bluefin tuna. *Nature*. **434**, 1121–1127 (2005).

50. M. S. Triantafyllou, G. S. Triantafyllou, An Efficient Swimming Machine. *Scientific American*. **272**, 64–70 (1995).

51. M. Kurt, J. Cochran-Carney, Q. Zhong, A. Mivehchi, D. B. Quinn, K. W. Moored, Swimming freely near the ground leads to flow-mediated equilibrium altitudes. *Journal of Fluid Mechanics*. **875**, R1 (2019).

52. G. Timmerhaus, C. C. Lazado, N. A. R. Cabillon, B. K. M. Reiten, L.-H. Johansen, The optimum velocity for Atlantic salmon post-smolts in RAS is a compromise between muscle growth and fish welfare. *Aquaculture*. **532**, 736076 (2021).

53. V. Di Santo, C. P. Kenaley, G. V. Lauder, High postural costs and anaerobic metabolism during swimming support the hypothesis of a U-shaped metabolism–speed curve in fishes. *Proceedings of the National Academy of Sciences*. **114**, 13048–13053 (2017).

54. P. He, C. S. Wardle, Tilting behaviour of the Atlantic mackerel, Scomber scombrus, at low swimming speeds. *Journal of Fish Biology*. **29**, 223–232 (1986).

55. K. Cathcart, S. Y. Shin, J. Milton, D. Ellerby, Field swimming performance of bluegill sunfish, Lepomis macrochirus: implications for field activity cost estimates and laboratory measures of swimming performance. *Ecology and Evolution*. **7**, 8657–8666 (2017).

56. E. D. Gellman, T. R. Tandler, D. J. Ellerby, Swimming from coast to coast: a novel fixed-gear swimming gait in fish. *Biology Letters*. **15**, 20190270 (2019).

57. N. W. Xu, J. O. Dabiri, Low-power microelectronics embedded in live jellyfish enhance propulsion. *Science Advances*. **6**, eaaz3194 (2020).

58. K. Y. Lee, S.-J. Park, D. G. Matthews, S. L. Kim, C. A. Marquez, J. F. Zimmerman, H. A. M. Ardoña, A. G. Kleber, G. V. Lauder, K. K. Parker, An autonomously swimming biohybrid fish designed with human cardiac biophysics. *Science*. **375**, 639–647 (2022).

59. M. B. S. Svendsen, P. G. Bushnell, J. F. Steffensen, Design and setup of intermittent-flow respirometry system for aquatic organisms. *Journal of Fish Biology*. **88**, 26–50 (2016).

60. Y. Zhang, thesis, University of British Columbia (2021).

61. R. J. Kline, D. C. Parkyn, D. J. Murie, Empirical Modelling of Solid-blocking Effect in a Blazka Respirometer for Gag, a Large Demersal Reef Fish. *Advances in Zoology and Botany*. **3**, 193–202 (2015).

62. Y. Zhang, G. Claireaux, H. Takle, S. M. Jørgensen, A. P. Farrell, A three-phase excess post-exercise oxygen consumption in Atlantic salmon Salmo salar and its response to exercise training. *J Fish Biol*. **92**, 1385–1403 (2018).

63. H. F. Wootton, J. R. Morrongiello, T. Schmitt, A. Audzijonyte, Smaller adult fish size in warmer water is not explained by elevated metabolism. *Ecology Letters*. **25**, 1177–1188 (2022).

64. D. Chabot, J. F. Steffensen, A. P. Farrell, The determination of standard metabolic rate in fishes. *Journal of Fish Biology*. **88**, 81–121 (2016).

65. J. C. Svendsen, C. Tudorache, A. D. Jordan, J. F. Steffensen, K. Aarestrup, P. Domenici, Partition of aerobic and anaerobic swimming costs related to gait transitions in a labriform swimmer. *Journal of Experimental Biology*. **213**, 2177–2183 (2010).

66. A. E. Brafield, D. J. Solomon, Oxy-calorific coefficients for animals respiring nitrogenous substrates. *Comparative Biochemistry and Physiology Part A: Physiology*. **43**, 837–841 (1972).

67. T. L. Hedrick, Software techniques for two- and three-dimensional kinematic measurements of biological and biomimetic systems. *Bioinspir. Biomim.* **3**, 034001 (2008).

68. M. Saadat, F. Berlinger, A. Sheshmani, R. Nagpal, G. V. Lauder, H. Haj-Hariri, Hydrodynamic advantages of in-line schooling. *Bioinspir Biomim*. **16** (2021), doi:10.1088/1748-3190/abe137.

69. F. E. Fish, C. A. Hui, Dolphin swimming–a review. *Mammal Review*. **21**, 181–195 (1991).

70. M. Daghooghi, I. Borazjani, The hydrodynamic advantages of synchronized swimming in a rectangular pattern. *Bioinspir. Biomim.* **10**, 056018 (2015).

Acknowledgments: Many thanks to members of Lauder Laboratory for numerous discussions about fish schooling behaviour, for comments on the manuscript, and to Cory Hahn for fish care.

Funding: Funding provided by the National Science Foundation grant 1830881 (GVL), the Office of Naval Research grants N00014-21-1-2661 (GVL), N00014-16-1-2515 (GVL), 00014-22-1-2616 (GVL), and a Postdoctoral Fellowship of Natural Sciences and Engineering Research Council of Canada PDF - 557785 – 2021 (YZ).

Author contributions:

Y.Z. and G.L. conceptualized the study. Y.Z. performed experiments and data analyses and wrote the manuscript. Y.Z. and G.L. provided manuscript edits and comments and approved the final version.

Competing interests: Authors declare that they have no competing interests.

Data and materials availability: All data generated or analysed during this study are included in this published article (and its supplementary information files).

Supplementary Materials:
Introductory text
Figs. S1 to S9
Tables S1 to S4

887 **TABLE HEADING**

888

889 **Table 1. A summary of experimental studies that directly estimate the energetic saving of**
890 **group movement in aerial and aquatic vertebrates that move through a fluid environment.**
891 No energetic measurements have made for freely-moving bird flocks. Three studies measured
892 the energetics of fish schools over a range of narrow speeds; two other studies measured the
893 energetics of fish schooling at one speed. But no studies have quantified *both* the aerobic and
894 anaerobic energetic cost of swimming as a group compared to solitary locomotion.

Animal group	Species	Testing speeds	Group size	Measurements	Results	Reference
Bird	*Pelecanus onocrotalus*	Voluntary flights	< 8	Heart rate	Group movement saves energy	Weimerskirch et al.,2001
Bird	*Columba livia*	Voluntary flights	6	Flap frequency & Accelerations	Group movement costs more energy	Usherwood et al.,2011
Bird	*Geronticus eremita*	Voluntary flights	14	Wing beat phase, spatial distribution	V-formation birds use phasing strategy to cope with wakes	Portugal et al., 2014
Ray-finned fish	15 species	1 speed, unknown speed	6–12 individuals	Aerobic energy	Grouping reduces metabolic rate	Parker, 1973
Ray-finned fish	*Notropis heterodon*	1 speed ~1.2 BL s^{-1}	3 individuals	Aerobic energy	Only schooling of 6 cm fish saves energy	Abrahams & Colgan, 1985*
Ray-finned fish	*Anguilla anguilla* L	6 speeds 1-2.2 BL s^{-1}	7 individuals	Aerobic energy	Schooling save energy at low speeds	Burgerhout et al.,2013*
Ray-finned fish	*Lepomis macrochirus* *Oncorhynchus mykiss*	4 speeds, 1.5-3 BL s^{-1}	1-8 individuals	Aerobic energy	Schooling saves energy	Currier et al., 2020*
Ray-finned fish	*Salmo salar*	6 speeds 1-3 BL s^{-1}	10 individuals	Aerobic energy	Schooling does not save energy	Hvas & Oppedal, 2019
Ray-finned fish	*Devario aequipinnatus*	14 speeds, 0.3–8 BL s^{-1}	8 individuals	Aerobic & anaerobic energy	Schooling saves energy at high speeds	Present study*

*Studies used group and individual fish in the same size swim-tunnel respirometer

†Other uncited studies of fish schoolings use kinematic calculations and computer simulation to indirectly show that fish schooling conserve energy

FIGURES & FIGURE CAPTIONS

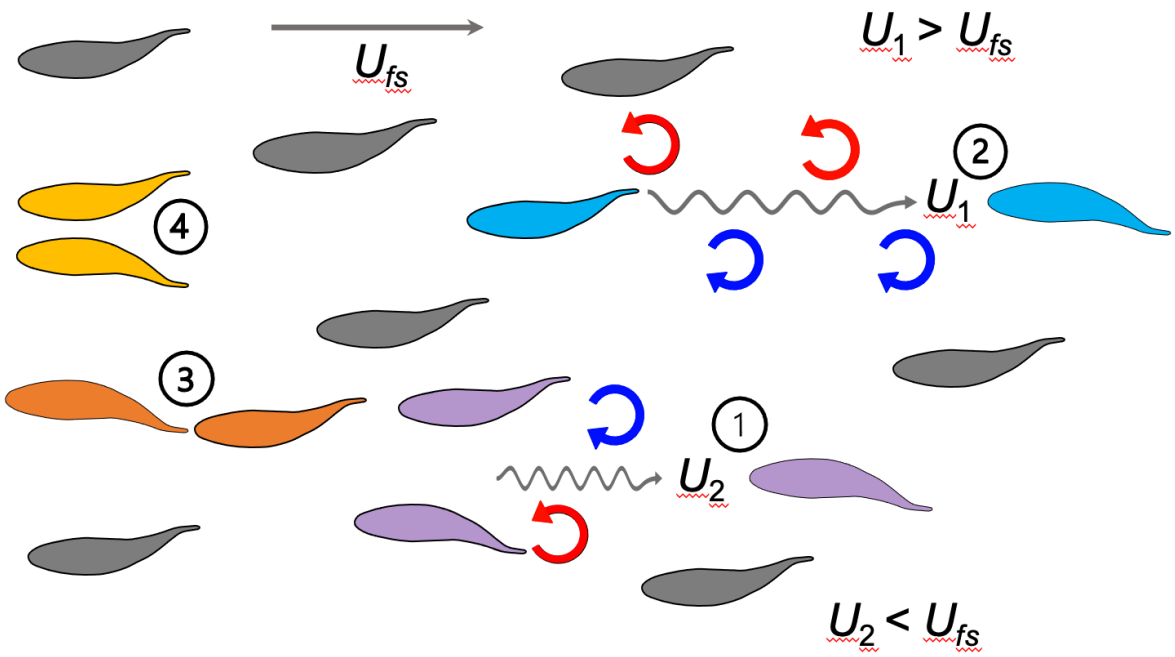

Fig. 1. A summary of biomechanical principles underlying proposed hydrodynamic advantages of schooling behaviour in fish. When fish swim into free-stream flow (U_{fs}), experimental data show that fish schools are dynamic with fish changing position frequently. Regardless of fish position within a school and changes in relative position, theoretical and robotic analyses have demonstrated at least four mechanisms (indicated by numbers) provide an advantage in the form of reduced power consumption. 1. Reduced oncoming velocity (U_2) requires less thrust for a fish swimming in the wake between two leading fish (*6*); 2. The Knoller-Betz effect of leading edge suction reduces costs for a trailing fish due to accelerated oscillating flow at the head (U_1) (*22*) (*67*); 3. Added mass "push" from follower to leader can reduce costs for the leader in front of another fish (*68*) (*21*) (*67*); 4. Wall effects benefit neighbouring fish where swimming next to another fish reduces swimming costs (*69*) (*18*). These principles suggest that regardless of the relative positions of the individuals within the fish school, the fish school as a collective unit should be able to save metabolic energy.

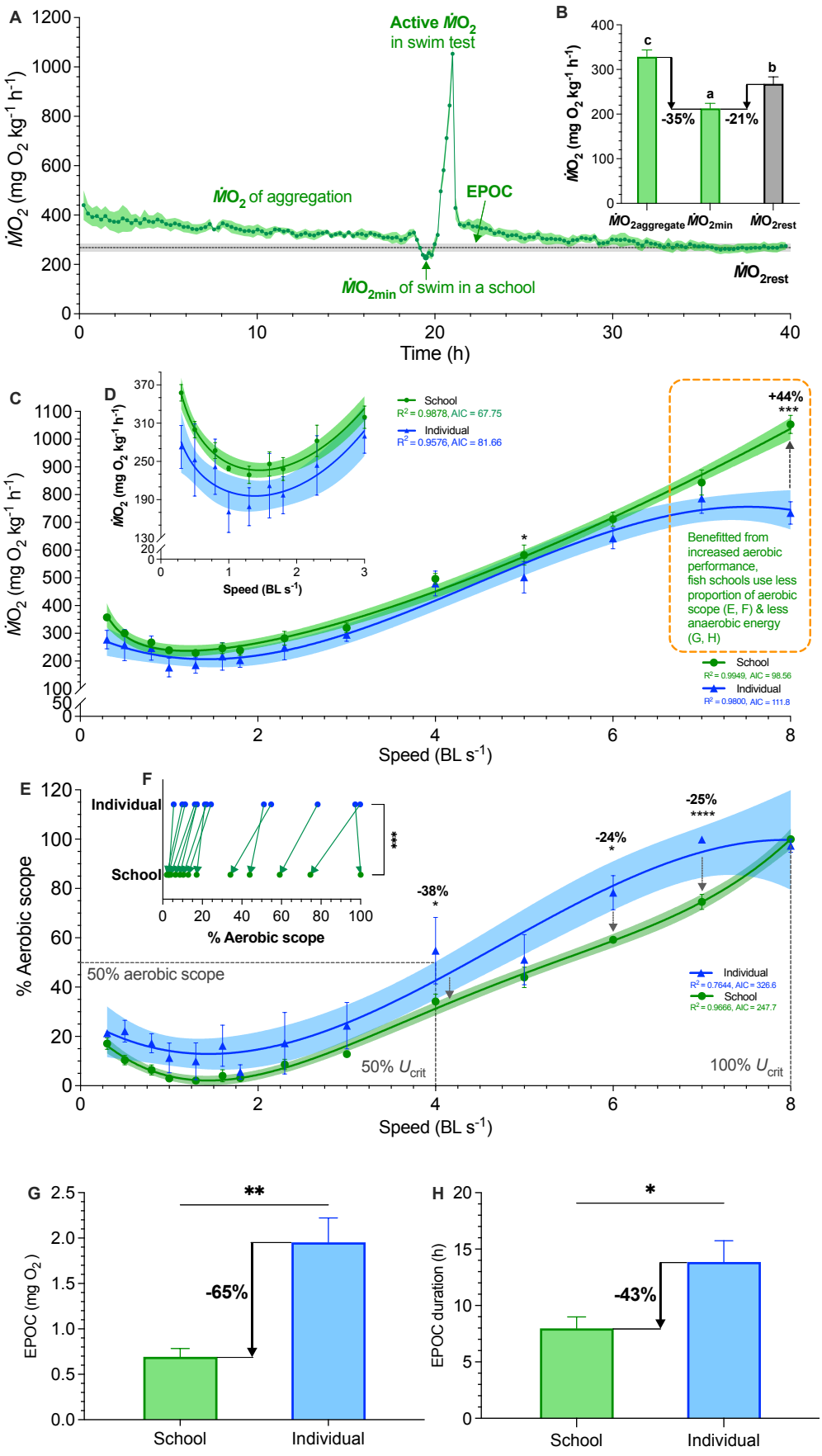
A
Active $\dot{M}O_2$ in swim test
$\dot{M}O_2$ of aggregation
EPOC
$\dot{M}O_{2min}$ of swim in a school
$\dot{M}O_{2rest}$
$\dot{M}O_2$ (mg O_2 kg^{-1} h^{-1})
Time (h)
B
c
a
b
-35%
-21%
$\dot{M}O_{2aggregate}$
$\dot{M}O_{2min}$
$\dot{M}O_{2rest}$
C
D
School
R^2 = 0.9878, AIC = 67.75
Individual
R^2 = 0.9576, AIC = 81.66
+44%
Benefitted from increased aerobic performance, fish schools use less proportion of aerobic scope (E, F) & less anaerobic energy (G, H)
School
R^2 = 0.9949, AIC = 98.56
Individual
R^2 = 0.9800, AIC = 111.8
Speed (BL s^{-1})
E
F
Individual
School
% Aerobic scope
-38%
-24%
-25%
50% aerobic scope
50% U_{crit}
100% U_{crit}
Individual
R^2 = 0.7644, AIC = 326.6
School
R^2 = 0.9666, AIC = 247.7
G
EPOC (mg O_2)
-65%
School
Individual
H
EPOC duration (h)
-43%
School
Individual

915

Fig. 2. Measurements of aerobic and anaerobic locomotor cost of fish schools and solitary fish. (**A**) Average traces of metabolic rate ($\dot{M}O_2$) of fish schools over a 40-hour experiment. Following the first 18-h quiescent state, a critical swimming speed (U_{crit}) test quantifies the aerobic cost of active swimming. The ensuing 18-h measurement of excess post-exercise oxygen consumption (EPOC) quantifies the anaerobic cost. (**B**) Comparison of $\dot{M}O_2$ for conditions of aggregating behaviour, minimum demand speed, and resting condition with the minimal flow ($\dot{M}O_{2aggregate}$, $\dot{M}O_{2min}$, $\dot{M}O_{2rest}$) (**C**) Comparisons of *J*-shaped $\dot{M}O_2$-speed curve over the entire range (0.3–8 body length s^{-1}, BL s^{-1}) and (**D**) *U*-shaped $\dot{M}O_2$-speed curve at the lower speeds (0.3–3 BL s^{-1}). (**E, F)** Percentage (%) aerobic scope used by fish schools and solitary fish during the U_{crit} test. (**G**, **H**) Comparisons of EPOC and EPOC durations between fish schools and solitary fish. Statistical significance is denoted by asterisk(s). Green colour = school data (n=5); blue colour = solitary fish data (n=5); shading indicates the 95% confidence interval. Statistical details are available in the statistical analyses section.

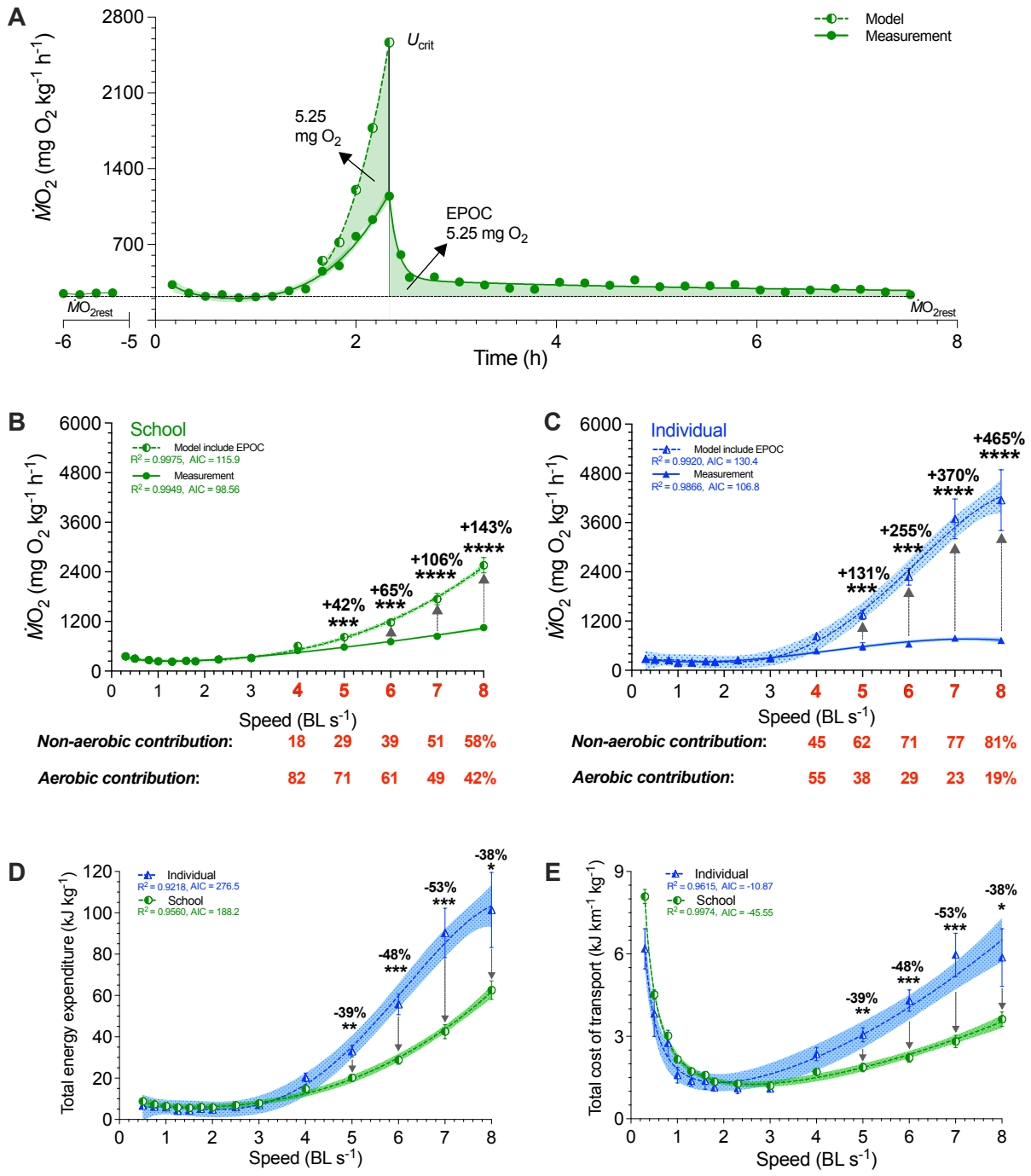
A
Model
Measurement
U_{crit}
5.25 mg O_2
EPOC 5.25 mg O_2
$\dot{M}O_2$ (mg O_2 kg^{-1} h^{-1})
$\dot{M}O_{2rest}$
Time (h)
B
School
Model include EPOC
R^2 = 0.9975, AIC = 115.9
Measurement
R^2 = 0.9949, AIC = 98.56
+42% ***
+65% ***
+106% ****
+143% ****
Speed (BL s^{-1})
Non-aerobic contribution: 18 29 39 51 58%
Aerobic contribution: 82 71 61 49 42%
C
Individual
Model include EPOC
R^2 = 0.9920, AIC = 130.4
Measurement
R^2 = 0.9866, AIC = 106.8
+131% ***
+255% ***
+370% ****
+465% ****
Non-aerobic contribution: 45 62 71 77 81%
Aerobic contribution: 55 38 29 23 19%
D
Individual
R^2 = 0.9218, AIC = 276.5
School
R^2 = 0.9560, AIC = 188.2
-39% **
-48% ***
-53% ***
-38% *
Total energy expenditure (kJ kg^{-1})
E
Individual
R^2 = 0.9615, AIC = -10.87
School
R^2 = 0.9974, AIC = -45.55
-39% **
-48% ***
-53% ***
-38% *
Total cost of transport (kJ km^{-1} kg^{-1})

929

930 **Fig. 3. Modeling of simultaneous aerobic and non-aerobic costs of fish schools and solitary**
931 **fish for a critical swimming speed (U_{crit}) test. (A)** Modeling the O_2 cost of the metabolic rate
932 ($\dot{M}O_2$)-speed curve and the ensuing recovery cost (excess post-exercise oxygen consumption,
933 EPOC) as a function of speed. After U_{crit}, fish returned to the same resting $\dot{M}O_2$ ($\dot{M}O_{2rest}$) as a
934 pre-test. (**B, C**) In addition to $\dot{M}O_2$ (solid line & filled symbols), we modeled the total O_2 cost
935 (dash line & half-filled symbols) for fish schools and solitary fish and when performing the U_{crit}
936 swimming test. The estimated partitioning of aerobic and non-aerobic contributions to swimming
937 are denoted (red-&-bold) with respect to speed for 4–8 BL s^{-1} is shown below each graph. (**D, E**)
938 Using total O_2 cost, we computed total energy expenditure (10-min period per point) and the
939 total cost of transport (including both aerobic metabolism, high-energy phosphate, and anaerobic
940 glycolysis) for both fish schools and solitary fish. Statistical significance is denoted by
941 asterisk(s). Green colour = school data (n=5); blue colour = solitary fish data (n=5); shading
942 indicates the 95% confidence interval. See methods for modeling and statistical details.

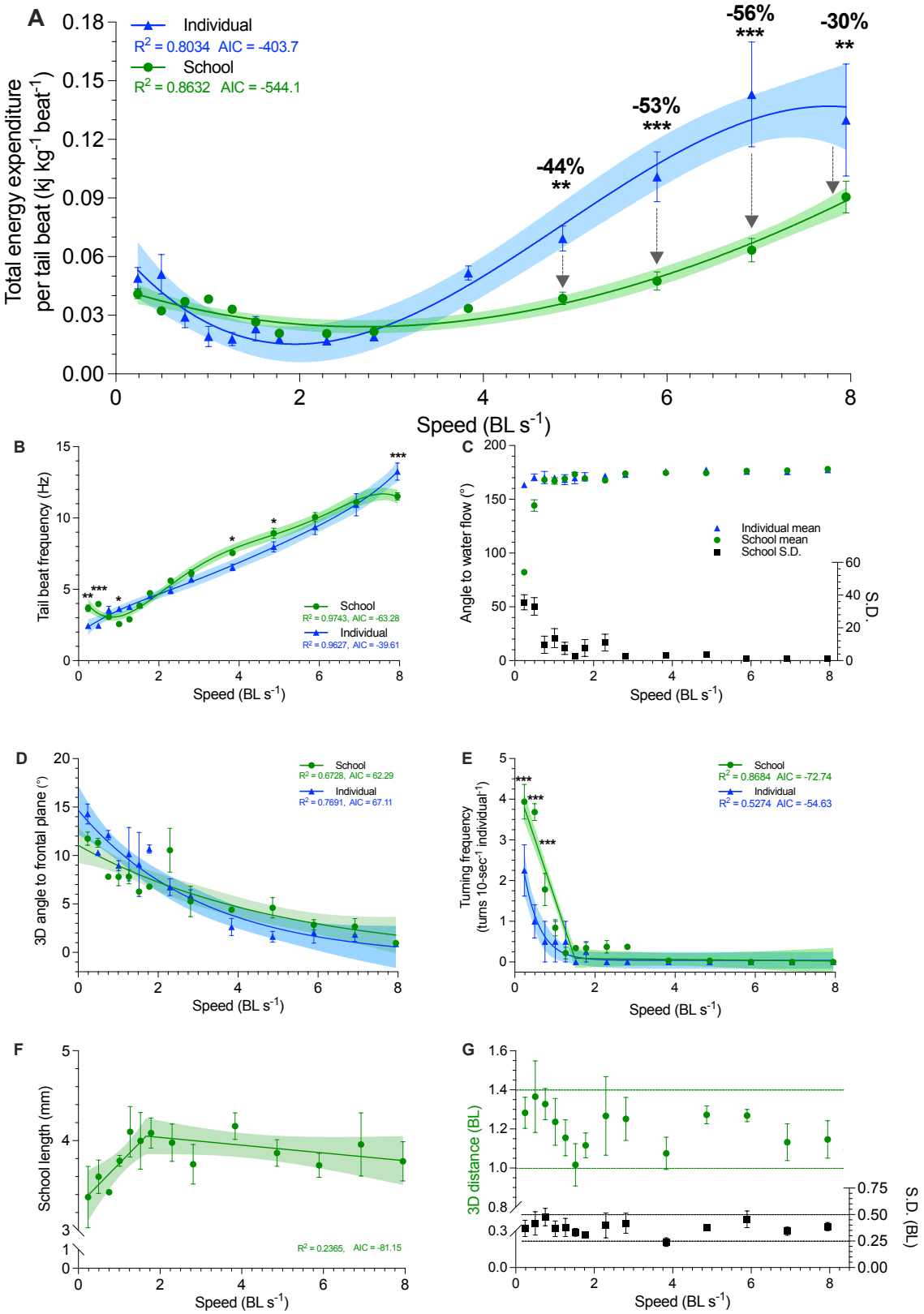
A
Individual
R² = 0.8034 AIC = -403.7
School
R² = 0.8632 AIC = -544.1
-44%
**
-53%
***
-56%
***
-30%
**
Total energy expenditure per tail beat (kj kg⁻¹ beat⁻¹)
Speed (BL s⁻¹)
B
Tail beat frequency (Hz)
School
R² = 0.9743, AIC = -63.28
Individual
R² = 0.9627, AIC = -39.61
Speed (BL s⁻¹)
C
Angle to water flow (°)
Individual mean
School mean
School S.D.
S.D.
Speed (BL s⁻¹)
D
3D angle to frontal plane (°)
School
R² = 0.6728, AIC = 62.29
Individual
R² = 0.7691, AIC = 67.11
Speed (BL s⁻¹)
E
Turning frequency (turns 10-sec⁻¹ individual⁻¹)
School
R² = 0.8684 AIC = -72.74
Individual
R² = 0.5274 AIC = -54.63
Speed (BL s⁻¹)
F
School length (mm)
R² = 0.2365, AIC = -81.15
Speed (BL s⁻¹)
G
3D distance (BL)
S.D. (BL)
Speed (BL s⁻¹)

943

944 **Fig. 4. Three-dimensional characterization of swimming kinematics and fish schooling**
945 **dynamics as a function of speed. (A)** Total energy expenditure per tail beat, (**B**) Tail beat
946 frequency, (**C**) The angle of fish to free-stream water flow, measured as the mean and the S.D. of
947 the angles of the individuals within the school. (**D**) Three-dimensional angle of fish to the frontal
948 plane. (**E**) Turning frequency, (**F**) Three-dimensional school length. (**G**) Three-dimensional
949 distances among all individuals in the school and the S.D. of the distance. The visual illustrations
950 of the upper and lower boundaries of the metrics are indicated. Statistical significance is denoted
951 by asterisk(s). Green colour = school data (n=3-4); blue colour = solitary fish data (n=3-4);
952 shading indicates the 95% confidence interval. See methods for details of three-dimensional
953 reconstruction and statistics.